Heliyon 9 (2023) e20874

Contents lists available at ScienceDirect

Heliyon

journal homepage: www.cell.com/heliyon

Silicone oils aided fabrication of paraffin wax coated super-hydrophobic sand: A spectroscopic study

K. Al-Mokhalelati [a,*], F. Karabet [a], A.W. Allaf [b,**], M. Naddaf [b], B. Assfour [b], A.G. Al Lafi [b]

[a] Department of Chemistry, Faculty of Science, Damascus University, Syrian Arab Republic
[b] Department of Chemistry, Atomic Energy Commission, Damascus, P.O.Box 6091, Syrian Arab Republic

ARTICLE INFO

Keywords:
Sand
Silicone oil
Paraffin wax
Super-hydrophobic sand
Fourier transform infrared spectroscopy
Molecular dynamic

ABSTRACT

To address the global alarm of desertification and boost plant progress in arid and desert environments, super-hydrophobic sand has been suggested and fabricated in numerous researches. In the present work, sand was hydrophobized by coating with a mixture of paraffin wax and silicone oils. The contact angle (CA) of sand with 4.5 w% silicone oils increased from 143.2° to 154.2° with decreasing the chain size of silicone oil, and the further addition of 13.5 w% of paraffin wax produced a super hydrophobic sand with a CA value up to 160° comparing to 154.2° without added paraffin wax. The Fourier Transform Infrared spectra suggested the development of inter molecular forces between silicone oil and sand as well as between paraffin and silicone oil, the driving force of which was the variation in viscosity of silicone oils. The later was higher in the case of lower molecular weight silicone oil. In particular, analyzing the characteristic bands of $-(CH_2)_n$-in paraffin wax, i.e. the corresponding bands at 720, 730, 1460 and 1470 cm^{-1} and the two bands at 1020 and 1095 cm^{-1} of silicone oil revealed that two roles of paraffin were taking place. While paraffin was placed between sand and silicone oil, it coated the sand particles when lower molecular weight silicone oil was used in the first procedures, whereas it coated the higher molecular weight silicone oil in the second procedures. Molecular dynamic calculation has been performed and confirmed the previous reached conclusions and showed that paraffin molecules were encapsulated in a silicone oil shell. The average adsorption energy of paraffin and silicon oil molecules on sand particles were 29.5 and 38.9 kcal mol^{-1} respectively.

1. Introduction

Arid and desert regions are expanded progressively causing severe ecological environment in desert, such as water shortage and sandstorm. Also, their extremely limited water sources, water pollution and water vanishing caused by evaporation and percolation have complicated the matter as well as the water stream to local, farming, and industrial districts [1]. The robust natural hydrophilicity of sand allowed the water to rapidly absorb and evaporate, which critically hinders desert greening, water storage and transportation strategies. However, owing to its low cost, environmentally friendly, superior chemical and thermal stabilities, and plentiful in the desert and seacoast, sand is an ideal inorganic material and a suitable candidate as an applicable substrate to construct

* Corresponding author.
** Corresponding author.
E-mail addresses: kamal7.almokhalelati@damascusuniversity.edu.sy (K. Al-Mokhalelati), aallaf@aec.org.sy (A.W. Allaf).

https://doi.org/10.1016/j.heliyon.2023.e20874
Received 16 April 2023; Received in revised form 8 September 2023; Accepted 9 October 2023
Available online 10 October 2023

super-hydrophobic surfaces materials. Therefore, many attempts have been suggested to hydrophobize sand utilizing diversities of production routes and hydrophobic materials. Artificial plastic mulches have been proven to minimize water losses, but their applications have been limited by their expensive installation, non-biocompatibility and their probable involvement in micro plastics contaminations [2,3]. Liu et al. fabricated super-hydrophobic sand materials aided by two routes; polymerizing the hydrochloride salt form of dopamine [4] and attaching SiO_2 nanoparticle onto the sand particles and modifying with hexadecyltrime-thoxysilane [5]. The wetting property expressed as the water contact angles has been reported to reach 153° and 163° respectively. Another promising approach to obtain super-hydrophobic sand with improved water-usage effectiveness for agricultural purposes has been achieved by modification of sand using engineered nanomaterials, including tetraethoxysilane (TEOS), trichloro (1H,1H,2H, 2H-perfluorooctyl) silane (PFOCTS), and a combination of them [1]. Moreover, Mosayebi et al. utilized chemical vapor deposition to load poly-dimethylsiloxane (PDMS) on the surface of sand grains for the use as effective filter for oil/water separation. The prepared super-hydrophobic sand possessed a water contact angle of 152° [6]. Among the materials that have been used to hydrophobized sand, purified paraffin waxes are inexpensive at an industrial scale, biodegradable, nontoxic, and safe for food industry [7,8]. Gallo Jr. et al. utilized dip coating method to produce paraffin-coated sand for water-management and agricultural purposes [9]. One the other hand, these coatings showed adhesion and mechanical instability problems, in addition to their relatively short service life [10]. To overcome these limitations, the present work was directed to incorporate silicone derivatives, such as silicone oils, that have been of interests due to their remarkable adhesion to solid surfaces such as glass and sand [11,12].

In the present work, sand was hydrophobized by coating with a mixture of paraffin wax and silicone oils having two different molecular weights. The materials properties of the coated sand were investigated focusing on the wetting properties, morphologies and structural alterations were probed by Fourier Transform Infrared spectroscopy. Computational calculations were also provided to reveal the structure of coated sand and explain the effects of silicone oils molecular weight.

2. Experimental

2.1. Materials and coating of sand

The materials specification details used in this work are quoted in Table 1 along with their chemical properties and sources.

To ensure homogeneity and reproducibility of the samples, the particles of natural and treated sand were characterized by scanning electron microscope (SEM). An average diameter of 200 μm was observed for natural sand, while the diameters of smashed sand particles ranged from 10 to 50 μm [8]. For each experiment, an amount of 10 g of treated sand was dispersed in 15 mL of n-hexane solution, which contains 0.5 g of selected silicone oil and varying amount of paraffin wax ranging from 0 to 2.5 g. The coated sand samples were produced by stirring these solutions at 150 rpm and a temperature of 50 °C using magnetic shaker until the solvent was evaporated. Two groups of samples were produced, as quoted in Table 2 to investigate the effects of chain size of silicone oils and added amounts of paraffin wax. Each group involved five sand-coated samples.

2.2. Characterizations

Fourier Transform Infrared (FTIR) spectroscopy (Nicolet 6700 FT-IR Spectrometer, Thermo Scientific, USA) functioned with a DTGS detector and the KBr sampling technique was utilized to probe any interaction between the components in the coated sand samples. All spectra were collected from 450 to 3800 cm^{-1} at a resolution of 2 cm^{-1} and 200 scans. A separate background spectrum was subtracted after each data collection.

X-ray diffraction (XRD)(STADI-P STOE, Darmstadt, Germany) equipped with CuK_α radiation ($\lambda = 1.54060\,\mathring{A}$) and a germanium monochromator was employed to explore crystallinity and chemical reaction between crystalline components in the coated sand samples. XRD patterns were recorded from $2\theta = 10°$ to $2\theta = 90°$ with a scanning step of 0.02°. A scanning electron microscope (SEM) (Tescan Vega II XMU, USA) operated at 20 kV was used to describe the morphology of coated sand samples.

The wettability characteristics of coated samples were evaluated by measuring the contact angles. This was carried out using the sessile drop method, an OCA 15 plus, SCA 20 (Data Physics Instrument GmbH, Germany) and an image analysis system. The coated sand samples of different compositions and groups were pressed at 1 ton to prepare circular discs of 1 cm in diameter, the contact angles were then measured by placing a double distilled water droplet (3 μL) onto each resulted disc. A minimum of triplicates were conducted for each sample, and the standard deviation was calculated for each.

Table 1
Materials used and their specifications.

Material	Properties		Source
Sand	Cleaned by water, dried at 50–65 °C, crashed and sieved to less than 90 μm.		Al-Qaryatayn, Homs city, the Syrian Desert
Paraffin wax	Melting point = 58–60 °C, C_nH_{2n+2}, n = 20–30		Avonchem, United Kingdom
silicone oil	$(CH_3)_3Si[OSi(CH_3)_2]_nOSi(CH_3)_3$	AK-350 (M_w = 6500, n = 110) AK-12500 (M_w = 40200, n = 500)	Wacker-Chemie GmbH, Germany
N-hexane	Boiling point = 69.0 °C		Sigma-Aldrich, Germany

Table 2
Samples designation and their composition.

Samples designation	Composition (w%)			
	Sand	Paraffin wax	AK-350	AK-12500
Group (I)	75.5–95.5	0–20	4.5	0
Group (II)			0	4.5

2.3. Computational details

To acquire a detailed insight about the adsorption process, a combined Grand Canonical Monte Carlo (GCMC)-molecular dynamic (MD) approach was applied [13]. Firstly, to find the best adsorption position for paraffin and silicone oil on SiO_2, GCMC technique was used. The GCMC has been successfully applied in many investigated systems to study the adsorption of several fluids in different solid surfaces, such as gases in organic-inorganic slit pores [14], hydrogen sulfide and carbon dioxide co-adsorption in organic and inorganic shale nonopores [15], and methane storage on nano-pores [16]. The results of GCMC simulations can provide valuable insights into the mechanisms and factors that control adsorption phenomena at the nanoscale level. The GCMC calculations was performed using RASPA simulation package [17]. The silicone oxide substrate was created using a detailed atomistic description, as had the paraffin and silicon oil molecules. Parameters for the atomic interactions were taken from the DREIDING force field [18].

To reach equilibrium, the simulations ran for 1 million steps, followed by another 1 million steps to collect data. During each Monte Carlo step, there were attempts to insert a new molecule, delete an existing one, or translate or rotate an existing molecule.

In the further step, MD simulations was performed. It preserves the dynamical information of the system and can capture the effects of molecular interactions and motions on the interest properties. The MD simulation was performed utilizing the dispersion-corrected density functional based tight binding theory (DC-DFTB) [19,20], as implemented in DFTB + simulation package [20]. After initial structure equilibration for 100 ps (ps) at 300 K with a 0.25 fs (fs) time step. Subsequently, the equations of motion were integrated for another 100 ps using the same time step**.** Throughout the simulation, the temperature (T) was controlled at 300 K via a Berendsen thermostat with a 0.1 constant, while the number (N) of atoms and the simulation volume (V) were controlled through a canonical (NVT) ensemble. This combined procedure of GCMC and MD enables the determination of the most favorable adsorption sites in a relatively unbiased routine [13]. The binding energy (E_b) between molecules and surface was calculate using the following equation: $E_b = E_{total} - (E_{molecule} + E_{SiO2\text{-}Surface})$.

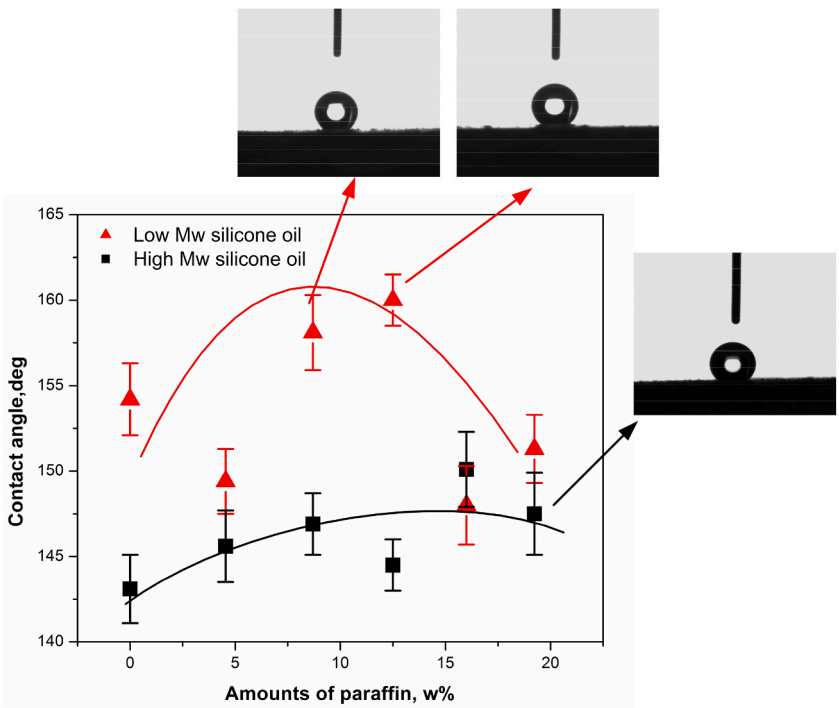

Fig. 1. The contact angle values as a function of paraffin content of coated sand, loading of silicone oil was constant at 4.5 %, and visual photos of a water droplet on a uniform surface of selected coated sand.

3. Results and discussion

3.1. Characterization of silicone oil/paraffin coated sand

Wetting properties of all samples were first evaluated by measuring their contact angles. Fig. 1 displays the values of water contact angle (CA) of two different molecular weight (Mw) silicone oil coated sand samples, and showing the synergy between paraffin wax and silicone oils for the preparation of super-hydrophobic sand. With respect to Mw of the used silicone oil, the CA increased from 143.2° to 154.2° with decreasing Mw. Even after the addition of paraffin wax, the CA values of coated sand were 10–12° higher in the lower Mw silicone oil coated sand (group I). Moreover, the addition of 13.5 w% of paraffin wax produced a super hydrophobic sand with a CA value of 160° comparing to 154.2° without added paraffin wax. Fig. 1 also shows that there was a well-defined trend with added paraffin for the higher Mw silicone oil (group II), while the data were more scattered and passing through a maximum for the lower Mw silicone oil. The images of water droplet on the surface of different coated sand shown in Fig. 1 confirmed the super-hydrophobic nature of the fabricated sand.

It was evident that silicone oil was more effective in hydrophopizing the sand than paraffin, but the combination of both paraffin and silicone oil produced the most super-hydrophobic sand, particularly, the system comprised paraffin: silicone oil of 3:1 in group I. In addition, the results indicated that there was an effect of the Mw of the used silicone oil, and AK-350 produced higher CA than AK-12500, and the synergetic effect of paraffin wax was much more pronounced with AK-350.

Similar super-hydrophobic behavior has been reported for hydrophobized sand surface coated with different materials as shown in Table 3. However, the simplicity and ease of fabrication of super-hydrophobic sand in the present work represent an advantege over other reported works.

The SEM pictures demonstrate that the particles of silicone oils coated sand, Fig. 2(a) and (d), were larger in the case of AK-350 with more broder size distribution. The accumulation of equal quantities of paraffin and silicone oils to the coating mixture increased the particle sizes as shown in Fig. 2(b) and (e). The further addtion of paraffin, Fig. 2(c) and (f) increased the particle sizes further and in particular for the AK-12500, while a distribution of sand particle size was observed with AK-350. The cosequences of such morphologies were the formation of voids that are filled with air and resulted in the hydrophobic nature of the coated sand.

Fig. 3(a–d) shows respectively the diffractograms for 100% sand, 100 % paraffin, 82 % sand with 13.5 % paraffin and 4.5 % low Mw silicone oil, and 82 % sand with 13.5 % paraffin and 4.5 % high Mw silicone oil samples. All samples were measured under the same conditions. The attributions of detected crystalline phases to the Bragg peaks were carried out based on the ICDD databank. Generally, sand contained solely the structure of the crystalline phase of silicone oxide (SiO_2), see Fig. 3(a), (Reference code: 01-077-1060). For paraffin, see Fig. 3(b), the phase that sensibly matched with the Bragg peaks was n-Paraffin $(CH_2)x$ (Reference code: 00-040-1995) [22–24]. Bucio et al. carried out a description of beeswax, camellia wax and paraffin wax for coating cheeses. The positions for paraffin identified by them are consistent with our findings [24].

Silicone oils were amorphous and did not change the XRD patterns of sand and paraffin. However, after the addition of paraffin wax, new peaks were observed at 21.42°, 23.80° and 26.6° that amplified with increasing paraffin: sand ratio and were assigned to paraffin wax [24]. It was noted that the intensity of paraffin wax patterns in the coated sand with AK-350, see Fig. 3(c) was lower than those in the coated sand with AK-12500, see Fig. 3(d), although all patterns were normalized based on the sand peak at 26.7°. This was attributed to the formation of more homogeneous mixture in the case of AK-350 due to its lower viscosity.

3.2. The FTIR spectra of sand, silicone oils and paraffin wax

The main absorption FTIR bands of sand occur at 3300–3500, 1600–1640, 1085, 800, 780, 695, 514 and 467 cm^{-1}, see Fig. 4. The region from 3300 to 3500 cm^{-1} is typical of the stretching mode of hydroxyl groups (-OH) situated at the surface (free water molecule), crystallized water, and silanol groups (Si–OH). The second region from 1600 to 1640 cm^{-1} is typical of the bending or deformation vibrations of coordinated water, which is adsorbed by the Si–O–Si structure [25,26]. These bands are informative, in particular, the intensity changes of –OH stretching vibration suggest modifications in the abundance of both silanol and water molecules, whereas the intensity changes of the H_2O bending vibration mode reveal a change in the quantity of molecular water present in the alteration layer [27]. A wide band located over the region from 1050 to 1100 cm^{-1}, with a center at 1085 cm^{-1}, is assigned to asymmetric stretching mode of Si–O–Si bonds. Widening of this region has been endorsed to lower order of the material, while a blue shift indicated the formation of Si–*O*-Metal bonds [28], and an absorption bands appeared at 1018 and 975 cm^{-1} have been assigned to the stretching modes of the Si–O–Al bonds [26]. The two absorption bands at 780 and 800 cm^{-1} have been assigned to Si–*O*–Si symmetrical

Table 3
Some reported coated system of sand and the corresponding CA value.

Super hydrophobic sand coated system	Contact angle (±1 deg)	Reference
TiO_2 or ZnO and monolayer of octyltrimethoxysilane	150	[21]
Paraffin waxcapsules and hydrophobic silica nanoparticles	165	[10]
Nanoscale wax coating	155	[9]
Tetraethoxysilane and perfluorodecyltrichlorosilane.	151	[1]
Chemical vapor deposition of polydimethylsiloxane	152	[6]
Dip coating in a mixture of silicone oil and paraffin	160	This work

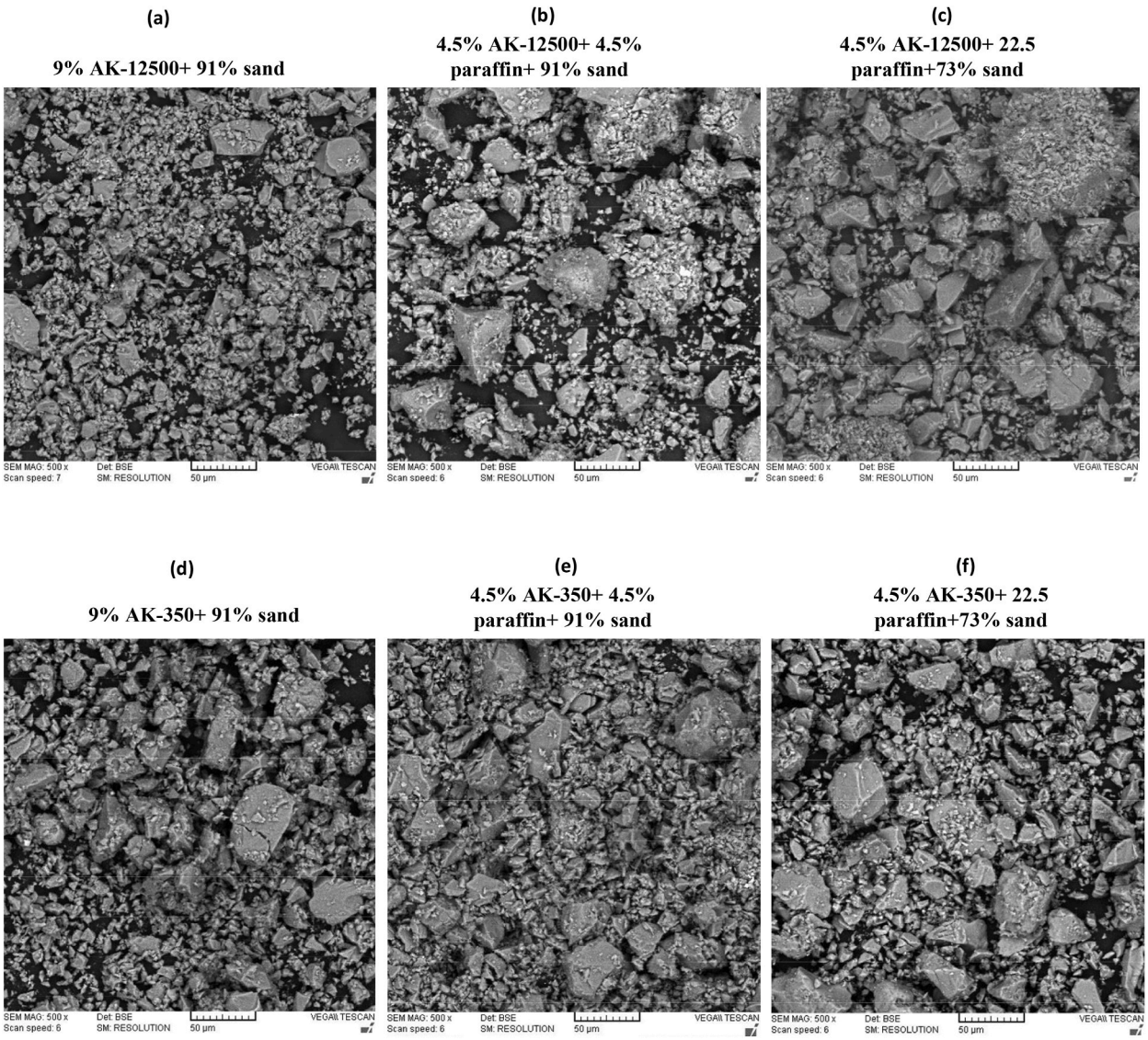

Fig. 2. The SEM images of different coated sand.

stretching modes in quartz. They varied according to the particle size, and confirmed the crystalline nature of silica [29]. The overlap of these two bands is minimum with particle size less than 2 µm [30], but they combined at 800 cm^{-1} with increasing particle size. Moreover, the previous bands have been verified as quantitatively the most appropriate bands of silica [25]. It is well known that two bands at 467 and 514 cm^{-1} are observed in many silicate materials [29]. The first band at 467 cm^{-1} is ascribed to Si–O–Si out of plane deformations while the second band at 514 cm^{-1} is assigned to the bending mode of O–Si–O [25,26]. The important band, which is observed at 695 cm^{-1}, has been assigned to symmetrical bending mode of Si–O in SiO_4, confirming the existence of crystalline quartz [23]. The intensity ratio 800/694 has been employed to estimate the crystallization degree of quartz based materials [31].

Whereas, the main FTIR bands of silicone oil used in the present work, see Fig. 5, are assigned based on the chemical structure shown in Table 1. The $–CH_3$ asymmetrical and symmetrical stretching modes appear near 2964 and 2905 cm^{-1} respectively. The band at 800 cm^{-1} has been ascribed to the coupling of the Si–C stretching mode and the $–CH_3$ rocking mode for the $Si–CH_3$ groups. The two broad FTIR bands near 1095 and 1020 cm^{-1} have been attributed to the Si–*O*–Si stretching mode of extended chain siloxanes. In addition, the strong and sharp band at 1260 cm^{-1} is ascribed to symmetrical deformation of $–CH_3$ in the $Si–CH_3$ group, while the weak band near 1410 cm^{-1} is assigned to asymmetrical deformation of $–CH_3$. The -$SiCH_3$ rock (in addition to probably some Si–C stretch interaction) infrared vibration bands were observed at 870-750 cm^{-1} [32–34]. No changes could be detected between FTIR spectra of AK-350 and AK-12500.

Moreover, the FTIR spectrum of paraffin wax is shown in Fig. 6 and is assigned as follow: the $–CH_3$ asymmetrical and symmetrical stretching modes wereobserved at 2962 and 2872 cm^{-1} respectively. They are of strong intensities, and their wavenumbers are

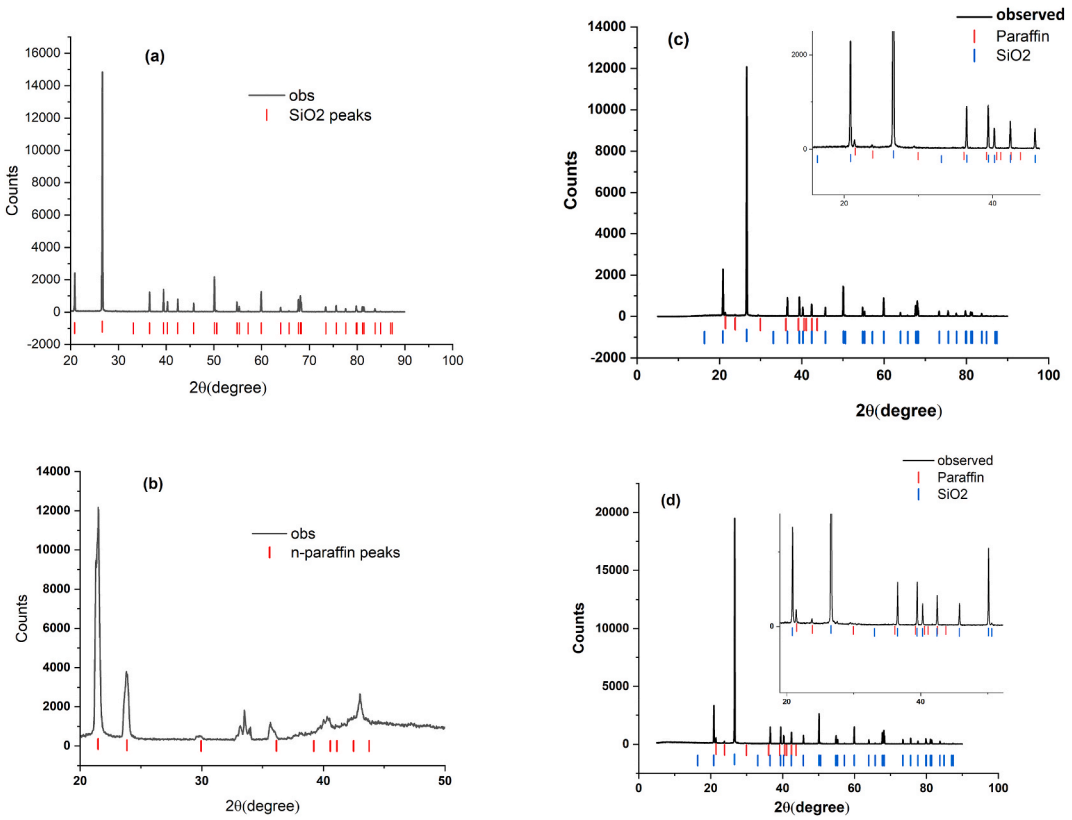

Fig. 3. The XRD patterns of sand (a), paraffin (b) and two coated sands with the same composition but different silicone oil grade: AK-350 (c) and AK-12500 (d).

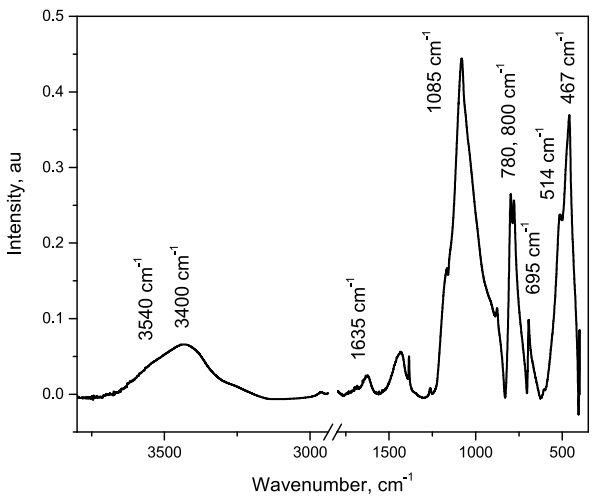

Fig. 4. The FTIR spectrum of typical sand material.

characteristic. The asymmetrical and symmetrical $–CH_2$ stretching modes appear as intense peaks at 2926 and 2853 cm^{-1}, respectively The asymmetrical and symmetrical $–CH_3$ bending modes occur at 1470–1430 and 1395-1365 cm^{-1} respectively. The 1380 cm^{-1} band does not overlap with other bands of alkanes and is usually indicative for the presence of $–CH_3$ on a carbon atom. The scissoring mode of the $–CH_2$ group appears near 1465 cm^{-1}. This band often overlaps with $–CH_3$ asymmetrical bending in the 1470-1430 cm^{-1} region. The band at 720 cm^{-1} is ascribed to the $-(CH_2)_n$-in-phase rocking mode. It appears in the FTIR spectrum as a medium to weak intensity band in the 726-720 cm^{-1} region when $n > 3$. In the crystalline solid state for long-chain $–CH_2$ groups, this band splits into a doublet at

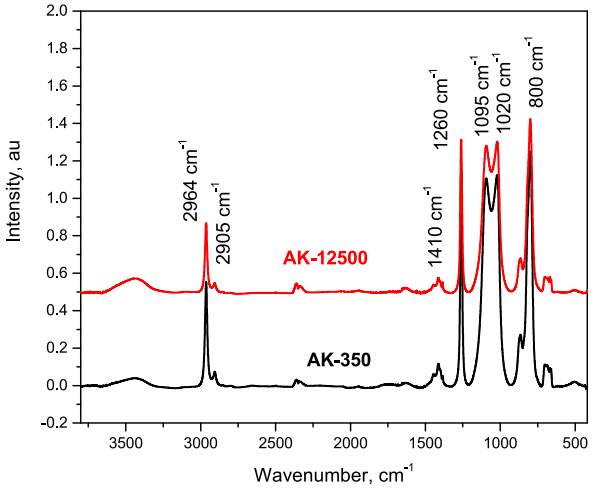

Fig. 5. The FTIR spectra of silicone oils.

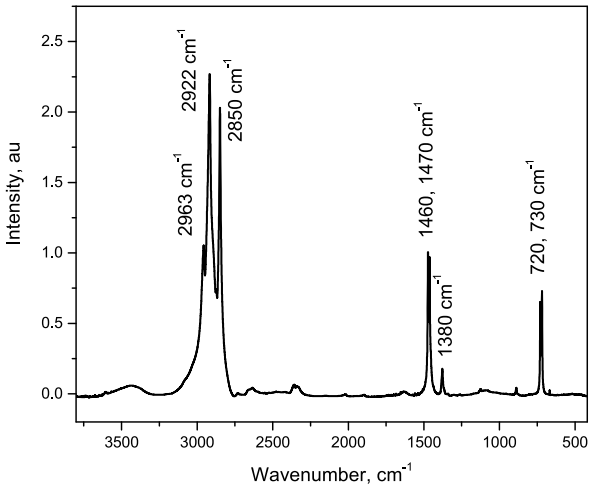

Fig. 6. The FTIR spectrum of paraffin wax.

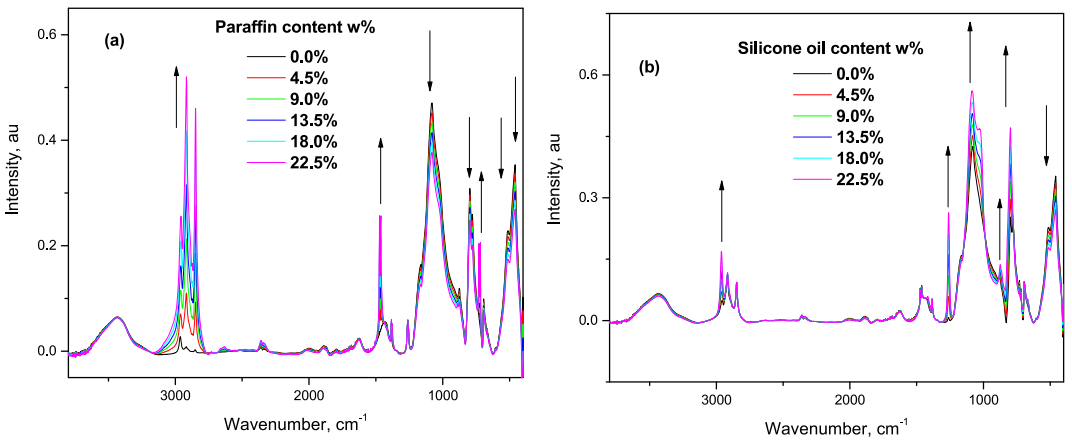

Fig. 7. The calculated FTIR spectra of coated sand: (a) increasing paraffin contents at a constant loading of silicone oil (AK-350), and (b) increasing silicone oil (AK-350) contents at a constant loading of paraffin. Upward arrows indicate the band that increase with increasing paraffin content (a) or increasing silicone oil (b), and downward arrows indicate bands that decrease with decreasing sand content.

730 and 720 cm^{-1}. The low intensity bands at 1080-1125 cm^{-1} has been attributed to C–C stretching mode. The band at 890 cm^{-1} has been assigned to methyl terminal rocking for $n > 10$ [35].

3.3. The FTIR spectra of coated sand

The FTIR spectra pointed out that each of the three components in the coated sand has well defined characteristic bands, that can be followed to probe the structural alterations occurred on making composition of these components. To capture these characteristic bands, the FTIR recorded spectra of the coated sand were calculated based on the experimentally measured FTIR spectra of each single component taking into consideration that the FTIR spectra are additive unless interactions between components had taken place [36].

Fig. 7(a) shows the calculated FTIR spectra of coated sand samples with increasing the amounts of paraffin wax from 0 to 22.5% at a fixed loading of 4.5 % of silicone oil (AK-350). Fig. 7(b) shows the calculated FTIR spectra of coated sand samples with increasing the amounts of silicone oil (AK-350) from 0 to 22.5% at a fixed loading of paraffin wax of 4.5 %. It was concluded that the bands at 2963, 1260, 875, 800 and 1020 cm^{-1} are characteristics of silicone oil, while the bands at 2915, 2850, 1460, 1470, 720 and 730 cm^{-1} are characteristics of paraffin. Moreover, the bands at 780, 514, 467 cm^{-1} are characteristics of sand. The calculated spectra were performed using Origin 7 pro software package utilizing the equation: calculated spectra = X (spectrum of sand) + Y (spectrum of paraffin) + Z (spectrum of silicon oil), where X, Y, and Z are the ratio of the corresponding component in the coated sand, and X + Y + Z = 100 %.

Moving to real experimental FTIR spectra as shown in Fig. 8. It was observed that the band at 2963 cm^{-1} in the FTIR spectra, which is characteristic of AK-350, Fig. 8(a), shifted to 2957 cm^{-1} after the addition of paraffin wax to the system. On the other hand, this band in the spectra of AK-12500, Fig. 8(b), shifted to 2960 cm^{-1} after the addition of the same amounts of paraffin. In addition, the strength of the band at 1263 cm^{-1} decreased after the addition of paraffin to both AK-350 and AK-12500 samples, but the reduction in intensity was more pronounced with AK-350. These indicated higher interaction between AK-350 and paraffin in comparison to AK-12500, probably due to the lower viscosity of the former enhancing the important role of viscosity.

Moreover, comparing the calculated spectra with the corresponding experimental ones, revealed that the characteristic bands for $-(CH_2)_n$-of paraffin wax, in particular the bands at 720, 730, 1460 and 1470 cm^{-1} appeared in the calculated spectra of both set of samples (Ak-350 and AK-12500) and increased in intensity with increasing the amounts of added paraffin. However, these bands appeared only in the FTIR spectra of group II, with lower intensity than expected. This indicated an interaction between paraffin wax and silicone oil probably by the formation of van der Waals' forces most likely Debby and London forces. The interaction was higher in group I in comparison with group II samples, as no such bands were observed. FTIR has been reported as a powerful tool to investigate intermolecular forces between H_2O and I_2 (Debby forces) [37], hydrogen bonds [38] and others [39].

Furthermore, both silicone oils have two bands at 1020 and 1095 cm^{-1}, that behaved similarly after the addition of sand. The band at 1020 cm^{-1} decreased in intensity, while the band at 1095 cm^{-1} moved to lower wavenumber at 1085 cm^{-1}. This indicated an increase in the intermolecular forces probably by the formation of intermolecular forces between sand and silicon oils. After the addition of paraffin wax to both systems, the intensity of the band at 1020 cm^{-1} decreased further and disappeared in the samples with AK-12500, while the band at 1085 cm^{-1} was not changed in both samples; with AK-350 and with AK-12500. As observed earlier, the sample with AK-350 and 9.0–13.5% paraffin wax produced the most super-hydrophobic sand.

Both silicone oils and paraffin wax are nonpolar, while sand is polar. Thus, it is expected that paraffin wax coated the silicone oils and in particular the high molecular weight one. This resulted in the disappearance of the band at 1020 cm^{-1}. In other words, paraffin breaks the intermolecular forces formed between sand and AK-12500, and located between sand and AK-12500. Paraffin played different role on the other coated group with AK-350. It is placed between sand and silicone oil and coats the sand, which stabilized and enhanced super-hydrophobic structure formation. The driving force of these differences was the variation in viscosity of silicone oils.

Generally, changes in the absorption ratio of two FTIR bands indicate a change in the chemical environments of the corresponding bands [40]. Fig. 9(a) and (b) show respectively, the calculated and experimental absorption ratio of 800/695 against the amounts of added paraffin wax in the coated sand. Both calculated and experimental data indicated that the changes were more pronounced with AK-350. The ratio 800/695 increased in the calculated spectra due to the reduction in sand, which resulted in decreasing the intensity of 695 cm^{-1} band. On the other hand, the reduction in the ratio 800/695 in the experimental spectra should be attributed to a reduction in the band intensity at 800 cm^{-1}. The drop in the intensity of the band at 800 cm^{-1} indicated the decreasing number of involving Si–*O*–Si bands that contributed to this band or to the decrease in polarity of the Si–*O*–Si bonds due to the formation of intermolecular forces between sand and paraffin wax.

The intensity ratio 800/695 has been employed to estimate the degree of crystallization of quartz based materials [31]. As the sand was not dissolved and re-crystallized, so the crystallinity in the FTIR indicated the orientation of bands or the crystallization of coating system components rather than sand as they were dissolved in n-hexane. In addition, the compositions of both groups of samples are similar; i.e. same silicone oil content, same sand and paraffin contents. Thus, the changes were attributed to interaction with paraffin and Mw of silicone oil. The addition of paraffin reduced the ratio 800/695 and increased the contact angle, while addition of silicone oils kept the added amount of paraffin wax at minimum.

3.4. Molecular dynamic of coated sand

Molecular simulations (MD) represent a way to study adsorption, as it affords detailed structural information, dynamics, and energetic of adsorbed systems. The MD simulations show that SiO_2 was stable with paraffin and silicone oil molecules adsorbed on it. Fig. 10 shows three different projections of the MD calculations along x (Fig. 10(a)), y (Fig. 10(b)) and z (Fig. 10(c)) axes respectively.

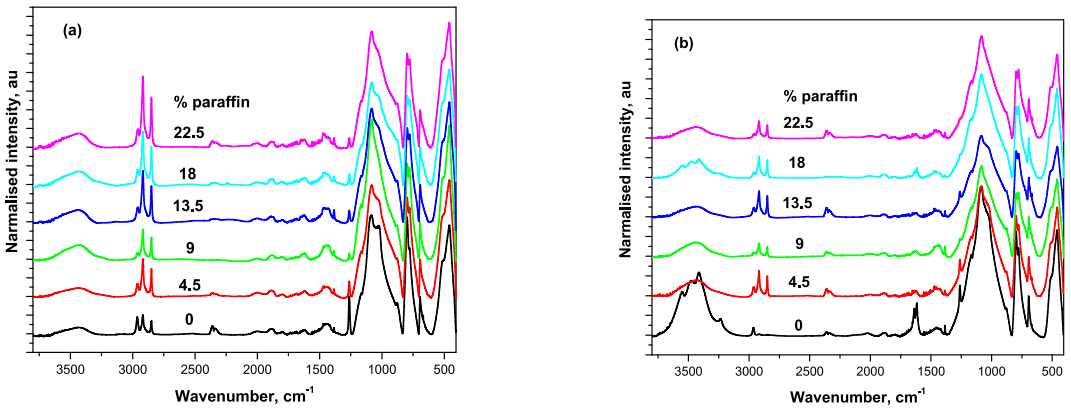

Fig. 8. The FTIR spectra of coated sand samples with emphasis on the effects of added paraffin wax and type of silicone oil: (a) AK-350 and (b) AK-12500.

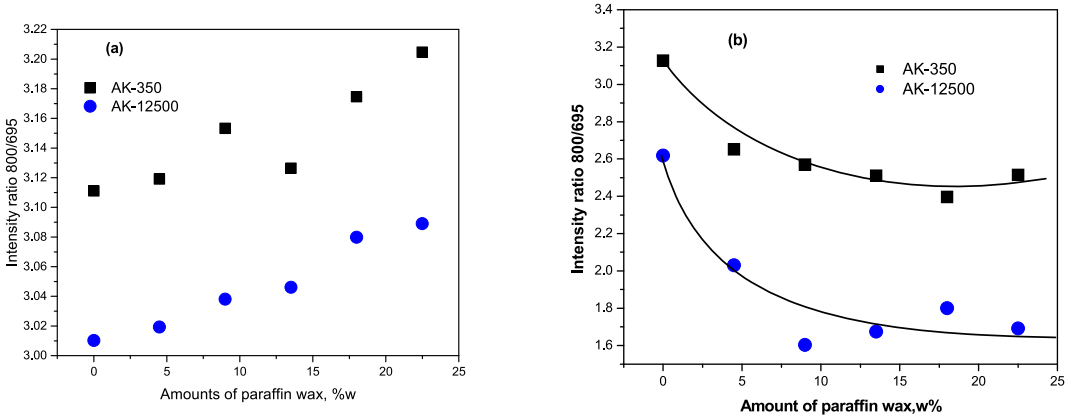

Fig. 9. The effects of paraffin wax on the calculated (a) and experimental (b) **intensity ratio** of **800/695**.

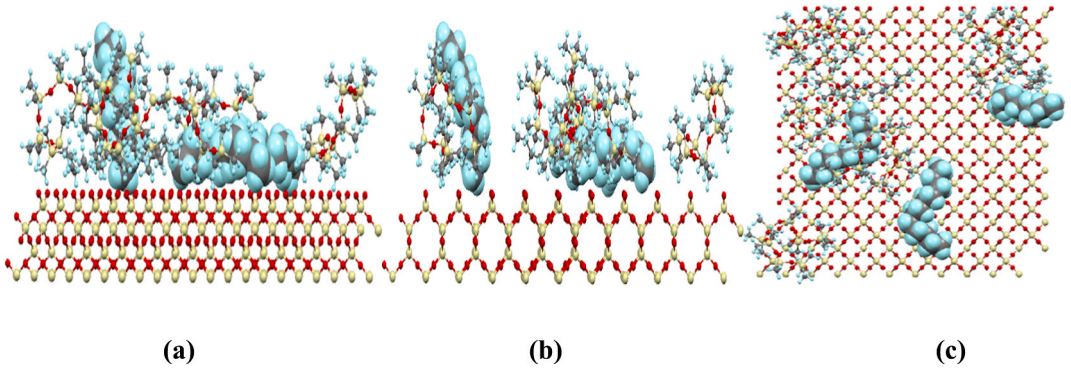

Fig. 10. The MD simulations results of paraffin and silicone oil molecules adsorbed on SiO_2 substrate: results projected along (a) x axe, (b) y axe and (c) the top view along z axe. For clarity, the paraffin molecules are shown as space fill. Si, yellow; O, red, C, black.

The results demonstrate that the paraffin can either adsorb vertically or parallel to the surface of the SiO_2. The paraffin molecules were encapsulated in a silicone oil shell, and there was no chemical reaction between them. The theoretical predicted adsorption mechanisms were in line with experimental results. The average adsorption energy of paraffin and silicone oil molecules on SiO_2 were 29.5 and 38.9 kcal mol^{-1}, respectively. This indicated that paraffin adsorbed on sand more favorably than silicone oil possibly due to its linear small size chains.

4. Conclusions

Super-hydrophobic sand was produced by a straightforward and fast procedure based on a mixture of silicone oil and paraffin wax. Paraffin wax was chosen for its desirable properties such as biodegradability, nontoxicity, and low price at an industrial scale, while silicone oils offer exceptional adhesion to sand surfaces. The contact angles reached 160° but decreased with increasing molecular weight of the silicone oils. Based on the FTIR analysis and molecular dynamic calculations, the coatings were physical in nature and two levels of intermolecular forces were formed between sand and paraffin as well as between paraffin and silicone oils. Lower molecular weight silicone oil was more effective and some molecules adsorbed on the surface of sand and synergize paraffin molecules to produce more super-hydrophobic sand with lower loading of paraffin. Understanding the mechanisms by which sand become super-hydrophobic revolutionize solution for arid land agriculture with insufficient water resources. FTIR spectroscopy combined with molecular dynamic calculations help to choose the right components and recipe to fabricate stable super-hydrophobic sand.

Data availability statement

The datasets generated during and/or analysed during the current study are available from the corresponding author on reasonable request.

Declaration of competing interest

The authors declare that they have no known competing financial interests or personal relationships that could have appeared to influence the work reported in this paper.

Acknowledgements

The authors thank Dr. G. Warkozek, the Director of Scientific Research at Damascus University, and Prof. I. Othman the General Director of Syrian Atomic Energy Commission, for their encouragements and supports.

References

[1] S.S. Ray, R. Soni, I.-C. Kim, Y.-I. Park, C.Y. Lee, Y.-N. Kwon, Surface innovation for fabrication of superhydrophobic sand grains with improved water holding capacity for various environmental applications, Environ. Technol. Innov. 28 (2022), 102849, https://doi.org/10.1016/j.eti.2022.102849.
[2] A. Paluselli, V. Fauvelle, F. Galgani, R. Sempéré, Phthalate release from plastic fragments and degradation in seawater, Environ. Sci. Technol. 53 (2019) 166–175, https://doi.org/10.1021/acs.est.8b05083.
[3] F. Shah, W. Wu, Chapter Five - use of plastic mulch in agriculture and strategies to mitigate the associated environmental concerns, Adv. Agron. 164 (2020) 231–287, https://doi.org/10.1016/bs.agron.2020.06.005.
[4] S. Liu, T. Cai, X. Shen, E. Huang, Z. Wang, Q. Sun, Superhydrophobic sand with multifunctionalities by TiO_2-incorporated mussel-inspired polydopamine, Ceram. Int. 45 (2019) 21263–21269, https://doi.org/10.1016/j.ceramint.2019.07.108.
[5] P. Liu, L. Niu, X. Tao, X. Li, Z. Zhang, Facile preparation of superhydrophobic quartz sands with micro-nano-molecule hierarchical structure for controlling the permeability of oil and water phase, Colloids Surf. A Physicochem. Eng. Asp. 569 (2019) 1–9, https://doi.org/10.1016/j.colsurfa.2019.02.035.
[6] E. Mosayebi, S. Azizian, N. Noei, Preparation of robust superhydrophobic sand by chemical vapor deposition of polydimethylsiloxane for oil/water separation, Macromol. Mater. Eng. 305 (2020), 2000425, https://doi.org/10.1002/mame.202000425.
[7] N.A. Adlan, S. Sabri, M. Masomian, M.S.M. Ali, R.N.Z.R.A. Rahman, Microbial biodegradation of paraffin wax in Malaysian crude oil mediated by degradative enzymes, Front. Microbiol. 11 (2020), 565608, https://doi.org/10.3389/fmicb.2020.565608.
[8] K. Al-Mokhalelati, F. Karabet, A.W. Allaf, M. Naddaf, A.G. Al-Lafi, Spectroscopic Investigations to Reveal Synergy between olystyrene Waste and Paraffin Wax in Super-hydrophobic Sand Scientific Reports, vol. 13, 2023, p. 9810, https://doi.org/10.1038/s41598-023-36987-4.
[9] A. G Jr., K. Odokonyero, M.A.A. Mousa, J. Reihmer, S. Al-Mashharawi, R. Marasco, E. Manalastas, M.J.L. Morton, D. Daffonchio, M.F. McCabe, M. Tester, H. Mishra, Nature-Inspired superhydrophobic sand mulches increase agricultural productivity and water-use efficiency in arid regions, ACS Agricultural Science & Technology 2 (2022) 276–288, https://doi.org/10.1021/acsagscitech.1c00148.
[10] A.M. Atta, M.M.S. Abdullah, H.A. Al-Lohedan, N.H. Mohamed, Coating sand with new hydrophobic and superhydrophobic silica/paraffin wax nanocapsules for desert water storage and transportation, Coatings 9 (2019) 124, https://doi.org/10.3390/coatings9020124.
[11] T. Mao, H. Feng, J. Wu, M. Li, S. Luo, J. Chen, X. Wei, P. Liu, F. Xie, Waterborne organic silicone polyurethane with excellent self-healing performance for oil/water-separation and oil-recovery applications, Sustainable Materials and Technologies 36 (2023), e00631, https://doi.org/10.1016/j.susmat.2023.e00631.
[12] A. Abbas, G.G. Wells, G. McHale, K. Sefiane, D. Orejon, Silicone oil-grafted low-hysteresis water-repellent surfaces, ACS Appl. Mater. Interfaces 15 (2023) 11281–11295, https://doi.org/10.1021/acsami.2c20718.
[13] O.F. Altundal, Z.P. Haslak, S. Keskin, Combined GCMC, MD, and DFT approach for unlocking the performances of COFs for methane purification, Ind. Eng. Chem. Res. 60 (2021) 12999–13012.
[14] J. Chen, F. Jiang, Q. Cong, X. Pang, K. Ma, K. Shi, B. Pang, D. Chen, H. Pang, X. Yang, Y. Wang, B. Li, Adsorption characteristics of shale gas in organic–inorganic slit pores, Energy 278 (2023), 127788, https://doi.org/10.1016/j.energy.2023.127788.
[15] M. Zhang, Z. Liu, B. Pan, S. Iglauer, Z. Jin, Molecular simulation on CO_2/H_2S co-adsorption in organic and inorganic shale nanopores, Appl. Surf. Sci. 624 (2023), 157167, https://doi.org/10.1016/j.apsusc.2023.157167.
[16] A. Sidorenkov, T. Aslyamov, D. Ilinov, M. Stukan, Methane storage in nano-pores: molecular dynamics simulation and density functional theory, Geoenergy Science and Engineering 222 (2023), 211419, https://doi.org/10.1016/j.geoen.2023.211419.
[17] D. Dubbeldam, S. Calero, D.E. Ellis, R.Q. Snurr, RASPA: molecular simulation software for adsorption and diffusion in flexible nanoporous materials, Mol. Simulat. 42 (2016) 81–101.
[18] S.L. Mayo, B.D. Olafson, W.A. Goddard, DREIDING: a generic force field for molecular simulations, J. Phys. Chem. 94 (1990) 8897–8909, https://doi.org/10.1021/j100389a010.
[19] L. Zhechkov, T. Heine, S. Patchkovskii, G. Seifert, H.A. Duarte, An efficient a posteriori treatment for dispersion interaction in density-functional-based tight binding, J. Chem. Theor. Comput. 1 (2005) 841–847, https://doi.org/10.1021/ct050065y.
[20] B. Hourahine, B. Aradi, V. Blum, F. Bonafé, A. Buccheri, C. Camacho, C. Cevallos, M.Y. Deshaye, T. Dumitrică, A. Dominguez, S. Ehlert, M. Elstner, T.v.d. Heide, J. Hermann, S. Irle, J.J. Kranz, C. Köhler, T. Kowalczyk, T. Kubař, I.S. Lee, V. Lutsker, R.J. Maurer, S.K. Min, I. Mitchell, C. Negre, T.A. Niehaus, A.M. N. Niklasson, A.J. Page, A. Pecchia, G. Penazzi, M.P. Persson, J. Řezáč, C.G. Sánchez, M. Sternberg, M. Stöhr, F. Stuckenberg, A. Tkatchenko, V.W.z. Yu,

T. Frauenheim, DFTB+, a software package for efficient approximate density functional theory based atomistic simulations, J. Chem. Phys. 152 (2020), 124101, https://doi.org/10.1063/1.5143190.
[21] Y. Liu, C.-H. Choi, Superhydrophobic sands for the preservation and purification of water, Coatings 11 (2021) 151, https://doi.org/10.3390/coatings11020151.
[22] N. Meftah, M.S. Mahboub, Spectroscopic characterizations of sand dunes minerals of el-oued (northeast Algerian sahara) by FTIR, XRF and XRD analyses, Silicon 12 (2020) 147–153, https://doi.org/10.1007/s12633-019-00109-5.
[23] N. Mahdadi, S. Chihi, H. Bouguettaia, S. Beddiaf, M.L. Mechri, Chromatic classification of ouargla (Algeria) dunes sand: determination of main compositions and color causes, by using XRD, FTIR and XRF, Silicon 9 (2017) 211–221, https://doi.org/10.1007/s12633-016-9432-x.
[24] A. Bucio, RosarioMoreno-Tovar, L. Bucio, J. Espinosa-Dávila, F. Anguebes-Franceschi, Characterization of bees wax, candelilla wax and paraffin wax for coating cheeses, Coatings 11 (2021) 261, https://doi.org/10.3390/coatings11030261.
[25] J. Ojima, Determining of crystalline silica in respirable dust samples by infrared spectrophotometry in the presence of interferences, J. Occup. Health 45 (2003) 94–103, https://doi.org/10.1539/joh.45.94.
[26] R. Ellerbrock, M. Stein, J. Schaller, Comparing amorphous silica, short-range-ordered silicates and silicic acid species by FTIR, Sci. Rep. 12 (2022), 11708, https://doi.org/10.1038/s41598-022-15882-4.
[27] H. Kaya, D. Ngo, S. Gin, S.H. Kim, Spectral changes in Si–O–Si stretching band of porous glass network upon ingress of water, J. Non-Cryst. Solids 527 (2020), 119722, https://doi.org/10.1016/j.jnoncrysol.2019.119722.
[28] M. Stein, A. Georgiadis, D. Gudat, T. Rennert, Formation and properties of inorganic Si-contaminant compounds, Environ. Pollut. 265 (2020), 115032, https://doi.org/10.1016/j.envpol.2020.115032 part B.
[29] P.L. Anderson, Free silica analysis of environmental samples-a critical literature review, Am. Ind. Hyg. Assoc. J. 36 (1975) 767–778, https://doi.org/10.1080/0002889758507338.
[30] E. Bye, G. Edholm, B. Gylseth, D.G. Nicholson, On the determination of crystalline silica in the presence of amorphous silica, Ann. Occup. Hyg. 23 (1980) 329–334, https://doi.org/10.1093/annhyg/23.4.329.
[31] J. Hlavay, K. Jonas, S. Elek, J. Inczedy, Characterization of the particle size and the crystallinity of certain minerals by IR spectrophotometry and other instrumental methods—II. Investigations on quartz and feldspar, Clay Clay Miner. 26 (1978) 139–143, https://doi.org/10.1346/CCMN.1978.0260209.
[32] S.I. Salih, J.K. Oleiwi, H.M. Ali, Study the mechanical properties of polymeric blends (SR/PMMA) using for maxillofacial prosthesis application, IOP Conf. Ser. Mater. Sci. Eng. 454 (2018), 012086, https://doi.org/10.1088/1757-899X/454/1/012086.
[33] J. Feng, Q. Zhang, Z. Tu, W. Tu, Z. Wan, M. Pan, H. Zhang, Degradation of silicone rubbers with different hardness in various aqueous solutions, Polym. Degrad. Stabil. 109 (2014) 122–128, https://doi.org/10.1016/j.polymdegradstab.2014.07.011.
[34] X. Wen, X. Yuan, L. Lan, L. Hao, Y. Wang, S. Li, H. Lu, Z. Bao, RTV silicone rubber degradation induced by temperature cycling, Energies 10 (2017) 1054, https://doi.org/10.3390/en10071054.
[35] R.M. Silverstein, F.X. Webster, D.J. Kiemle, Spectrometric Identification of Organic Compounds, seventh ed., John Wiley & Sons, Inc., USA, 2005.
[36] A.G. Al-Lafi, J.A. Abdullah, Y. Amin, Y. Aljbai, H. Allham, A. Obiad, The effects of pH on U(VI)/Th(IV) and Ra(II)/Ba(II) adsorption by polystyrene-nano manganese dioxide composites: Fourier Transform Infra-Red spectroscopic analysis, Spectrochim. Acta Mol. Biomol. Spectrosc. 267 (2022), 120588, https://doi.org/10.1016/j.saa.2021.120588. Part 2.
[37] A.G. Al-Lafi, B. Assfour, T. Assaad, Metal organic framework MIL-101(Cr): spectroscopic investigations to reveal Iodine capture mechanism, J. Inorg. Organomet. Polym. Mater. 30 (2020) 1218–1230, https://doi.org/10.1007/s10904-019-01236-7.
[38] A.G. Al-Lafi, J.A. Abdullah, Y. Amin, G. Alsayes, N. Al-Kafri, The effects of pH on the structure of polystyrene-nano manganese dioxide composites, J. Mol. Struct. 1237 (2021), 130315, https://doi.org/10.1016/j.molstruc.2021.130315.
[39] L.J. Bellamy, The Infrared Spectra of Complex Molecules, V-2 Advances in Infrared Group Frequencies, 2 ed., Chapman & Hall, London, 1980.
[40] A.G. Al-Lafi, J.N. Hay, 2D-COS-FTIR analysis of high molecular weight poly (N-vinyl carbazole) undergoing phase separation on purification and thermal annealing, J. Mol. Struct. 1175 (2019) 152–162, https://doi.org/10.1016/j.molstruc.2018.07.077.